

Optical Saturation in Fluorescence Correlation Spectroscopy under Continuous-Wave and Pulsed Excitation

Ingo Gregor,^[b] Digambara Patra,^[a] and Jörg Enderlein*^[a]

A detailed theoretical and experimental study of the dependence of fluorescence correlation measurements on optical excitation power due to optical saturation effects is presented. It is shown that the sensitivity of a fluorescence correlation measurement on excitation power becomes increasingly stronger for decreasing

excitation power. This makes exact measurements of diffusion coefficients with fluorescence correlation spectroscopy rather difficult. A strong difference of this behavior for continuous-wave and pulsed excitation is found.

Introduction

Fluorescence correlation spectroscopy (FCS) was originally introduced by Elson, Magde, and Webb in the early seventies^[1–3] and has seen a tremendous revival of attention over the last decade. Today, FCS has become an important spectroscopic technique, which is used in numerous biophysical studies and has many applications in analytical chemistry and biochemistry. Excellent introductions and overviews to FCS can be found in the literature.^[4–6] For recent reviews, see refs. [7–9].

In a typical FCS measurement setup, a laser is focused, by an objective with high numerical aperture (NA), into a sample solution containing fluorescing molecules at low concentration (less than one molecule within the detection volume). Fluorescence is collected through the same objective and separated from the excitation light via a dichroic mirror, which is reflecting at the laser's wavelength and transmitting for the Stokes-shifted fluorescence emission. The collected fluorescence is focused onto a circular confocal aperture and, behind that aperture, refocused onto a sensitive light detector, usually a single-photon-counting single-photon avalanche diode (SPAD). In FCS analysis, the recorded fluorescence intensity signal is correlated with a time-shifted replica of itself at different values of the lag time t . The result is the so-called autocorrelation function (ACF, second-order correlation function) $g(t)$ [Equation (1)]:

$$g(t) = \langle I(t_0)I(t_0 + t) \rangle \quad (1)$$

where $I(t)$ is the detected fluorescence intensity at time t , and the angle brackets symbolize averaging over all time values t_0 . On different time scales, the temporal behavior of the autocorrelation function is determined by different properties of the fluorescing molecules: On a microsecond time scale, $g(t)$ is dominated by triplet-state dynamics, photoisomerization, or similarly fast photophysical and photochemical processes. On a timescale of milliseconds to seconds, the autocorrelation function shows a typical decay due to translational diffusion of the molecules out of the detection region. Herein, the focus is on the diffusion-related temporal decay of the autocorrelation, which can be used to determine the diffusion coefficient of

the fluorescing molecules in solution and/or determine the fluorophore concentration in solution. Both values can be used to study molecular binding and unbinding,^[10–12] or chemical reaction kinetics.^[13–15]

The exact shape of the diffusion-related temporal decay of the autocorrelation function is solely determined by the shape of the molecule-detection function (MDF). The MDF quantifies the efficiency of detecting a fluorescence photon from a fluorescing molecule at a given position in sample space. The absorption dipole orientation of molecules with a rotational diffusion time which is much faster than the fluorescence lifetime is statistically independent of their emission dipole orientation. Then, the MDF is given by the direct product of the excitation probability distribution (EPD) times the light-collection efficiency function (CEF). If the excitation-light intensity is everywhere much below optical saturation, the EPD will be directly proportional to the excitation intensity distribution (EID), and the MDF will be equal to the product of the EID and the CEF. There is an extensive body of publications that deal with the impact of high-intensity excitation on confocal fluorescence microscopy, both in one- and multiphoton excitation regimes (see e.g., refs. [16–18]). The topic usually discussed in relation to high excitation intensities is photobleaching, which shifts the autocorrelation to shorter times. Surprisingly, a largely overlooked fact is that, often, the excitation intensity in the laser focus reaches values at which optical saturation becomes an important issue, which leads to a flattening of the excitation probability distribution in comparison to the excitation intensity distribution; this results in a virtually enlarged detection region and, thus, in apparently longer diffusion times and

[a] Dr. D. Patra, Dr. J. Enderlein
Institute for Biological Information Processing 1
Forschungszentrum Jülich, 52425 Jülich (Germany)
Fax: (+49) 2461-61-8069
E-mail: j.enderlein@fz-juelich.de

[b] Dr. I. Gregor
Institute for Biological Information Processing 2
Forschungszentrum Jülich, 52425 Jülich (Germany)

higher concentrations. This sensitive dependence of FCS measurements on excitation intensity was recently predicted in a theoretical study^[19] and extensively studied, both experimentally and by Monte Carlo simulations.^[20] For two-photon excitation, the enlargement of the MDF and its consequences for two-photon FCS has been discussed in detail.^[21] Herein, we report further on the significant power dependence of FCS measurements, considering the general case of pulsed, one-photon excitation. Pulsed excitation is often used for obtaining, simultaneously with FCS, information about fluorescence lifetimes via time-correlated single-photon counting.^[22,23] It will be shown that, even excitation with moderately short pulses—with pulse durations of some dozen picoseconds—leads to a dramatic increase in the power dependence of an FCS measurement.

Theory

Calculating the Autocorrelation Function

At any moment in time, the measured fluorescence intensity $I(t)$ is the sum of the individual contributions of all molecules in the sample, as shown in Equation (2):

$$I(t) = \sum_j I_j(t) \quad (2)$$

Assuming that all molecules have similar fluorescence properties, the autocorrelation function is then given by Equation (3):

$$g(t) = c \langle I_1(t)I_1(0) \rangle + c^2 \langle I_1 \rangle^2 \quad (3)$$

where c is the chemical concentration of fluorescing molecules (in number of molecules per unit volume), and I_1 stands for any single-molecule fluorescence contribution. The angle brackets denote averaging over all possible initial positions and diffusion paths of a single molecule, so that the two averages in the last equation are explicitly described by Equations (4) and (5):

$$\langle I_1(t)I_1(0) \rangle = \kappa \int d\mathbf{r}_1 \int d\mathbf{r}_0 U(\mathbf{r}_1) G(\mathbf{r}_1 - \mathbf{r}_0, t) U(\mathbf{r}_0) \quad (4)$$

$$\langle I_1 \rangle = \kappa \int d\mathbf{r} U(\mathbf{r}) \quad (5)$$

where $U(\mathbf{r})$ is the MDF, and $G(\mathbf{r}_1 - \mathbf{r}_0, t)$ denotes Green's function for the diffusion equation in free space, that is [Equation (6)]:

$$G(\mathbf{r}_1 - \mathbf{r}_0, t) = \frac{1}{(4\pi Dt)^{3/2}} \exp\left[-\frac{(\mathbf{r}_1 - \mathbf{r}_0)^2}{4Dt}\right] \quad (6)$$

Thus, if the MDF $U(\mathbf{r})$ is exactly known, it is straightforward to compute the exact autocorrelation function via the integrals involved in Equation (3).

The MDF is, for a quickly rotating molecule with negligible statistical correlation between its orientations during excitation and emission, given by the product of the probability of exciting the molecule times the CEF of collecting an emitted photon. The excitation probability distribution is itself a function of the excitation intensity distribution of the focused laser beam. For molecules with no optical saturation, the EPD is directly proportional to the EID; in the case of optical saturation, the relation between both functions is more complex (see below). Herein, the EID will be described by the simplified model of a scalar Gaussian laser beam [Equation (7)]:

$$\text{EID}(\rho, z) \propto \frac{1}{w^2(z)} \exp\left[-\frac{2\rho^2}{w^2(z)}\right] \quad (7)$$

where ρ is the radial co-ordinate $\rho = \sqrt{x^2 + y^2}$, and the position-dependent beam diameter $w(z)$ is given by Equation (8):

$$w(z) = w_0 \sqrt{1 + \left(\frac{z\lambda_{\text{ex}}}{\pi w_0^2}\right)^2} \quad (8)$$

where λ_{ex} is the wavelength of the laser light, and w_0 is the beam waist diameter.

For calculating the CEF, a semigeometrical optical approach can be used,^[24] which results in Equation (9a):

$$\text{CEF}(\rho, z) = \begin{cases} 0 & , \rho \geq R + a \\ \max(a, \omega)^2 (\theta_1 a^2 + \theta_2 R^2 - \Delta) / (\pi \omega^2 R^2) & , |R - a| < \rho < R + a \\ \max(a, \omega)^2 / \max(a, R)^2 & , \rho \leq |R - a| \end{cases} \quad (9a)$$

where the abbreviations $R = R(z)$, ω , $\theta_{1,2}$, and Δ are defined by Equations (9b)–(9f):

$$R(z) = \omega \sqrt{1 + \left(\frac{z\lambda_{\text{em}}}{\pi \omega^2}\right)^2} \quad (9b)$$

$$\omega = \frac{\lambda_{\text{em}}}{\pi \tan \Theta} \quad (9c)$$

$$\theta_1 = \arccos\left[\frac{a^2 + \rho^2 - R^2}{2a\rho}\right] \quad (9d)$$

$$\theta_2 = \arccos\left[\frac{R^2 + \rho^2 - a^2}{2R\rho}\right] \quad (9e)$$

$$\Delta = \frac{\sqrt{(a + \rho + R)(-a + \rho + R)(a - \rho + R)(a + \rho - R)}}{2} \quad (9f)$$

where λ_{em} is the center wavelength of fluorescence emission, Θ is the maximum angle of light collection defined by the objective's numerical aperture NA and the refractive index of the immersion medium n as $\sin \Theta = \text{NA}/n$, and a is the radius of the confocal aperture divided by the magnification of the optics. It has been shown^[24] that this CEF is an excellent ap-

proximation of the exact wave-optically calculated CEF obtained within the framework of scalar electrodynamics.

Because both the CEF and the EID (and thus also the EPD) show cylindrical symmetry, the resulting MDF (the product of CEF and EPD) is also cylindrically symmetric and only a function of ρ and z . In such a case, the three-dimensional integrals can be simplified by explicitly performing integration over the angular variable $\phi = \arctan(y/x)$, which results in Equation (10):

$$\langle I_1(t) | I_1(0) \rangle = \frac{2\pi\kappa}{(4\pi Dt)^{3/2}} \int_{-\infty}^{\infty} dz_1 \int_0^{\infty} d\rho_1 \rho_1 U(\rho_1, z_1) \left\{ \int_{-\infty}^{\infty} dz_0 \int_0^{\infty} d\rho_0 \rho_0 J_0 \left(\frac{i\rho_1 \rho_0}{2Dt} \right) \exp \left[-\frac{(\rho_1^2 + \rho_0^2) + (z_1 - z_0)^2}{4Dt} \right] U(\rho_0, z_0) \right\} \quad (10)$$

where J_0 is Bessel's function of zero order.^[25] This last expression involves only two two-dimensional integrals which can be easily handled numerically.

Optical Saturation under Pulsed Excitation

A largely underestimated fact is that the excitation probability is not only dependent on the excitation-light distribution in the sample but also on the molecule's photophysics and the mode of excitation. Let us consider a simple, three-state model of a fluorescing molecule, which consists of the ground state S_0 , the first excited singlet state S_1 , and the first triplet state T_1 . Neglecting photobleaching, the sum of the probabilities of finding the molecules in each of these three states will add to unity. Also, for most molecules, the $S_1 \rightarrow S_0$ transition rate is much faster than the intersystem crossing rate k_{isc} from S_1 to T_1 . Then, in a first approximation, one will only consider the fast cycling of the molecule between the S_0 and S_1 states while assuming that the sum of both populations remains constant and equals some value $s_{tot} = 1 - t_1 \leq 1$. For a constant excitation rate k_{ex} , the kinetic equation for the s_0 population probability is given by Equation (11):

$$\frac{ds_0(t)}{dt} = -k_{ex}s_0(t) + k_{10}[s_{tot} - s_0(t)] \quad (11)$$

where k_{10} is the return rate from the excited to the ground state (\approx inverse fluorescence lifetime). The explicit solution to that differential is Equation (12):

$$s_0(t) = \frac{k_{10}s_{tot}}{k_{10} + k_{ex}} \{ 1 + \alpha \exp[-(k_{ex} + k_{10})t] \} \quad (12)$$

where α is a constant that determines the value of s_0 at time zero. As a simplified model for a pulsed excitation, let us consider a periodic train of rectangular pulses of length T_{pulse} yielding a constant excitation rate k_{ex} and having a repetition period of T_{rep} . If $t=0$ is at the beginning of one of the pulses, then the evolution of s_0 for $0 \leq t \leq T_{pulse}$ is given by Equa-

tion (12), and after the pulse ($T_{pulse} \leq t \leq T_{rep}$) by the corresponding relation, Equation (13):

$$s_0(t) = s_{tot} \{ 1 - \beta \exp[-k_{10}(t - T_{pulse})] \} \quad (13)$$

where β is a constant that determines the value of s_0 at time $t = T_{pulse}$. Under steady-state conditions, that is, if s_0 adopts the same value after a full repetition period of length T_{rep} , one thus has Equations (14) and (15), which define the values of α and β :

$$\frac{k_{10}s_{tot}}{k_{10} + k_{ex}} \{ 1 + \alpha \exp[-(k_{ex} + k_{10})T_{pulse}] \} = s_{tot}(1 - \beta) \quad (14)$$

$$\frac{k_{10}s_{tot}}{k_{10} + k_{ex}} (1 + \alpha) = s_{tot} \{ 1 - \beta \exp[-k_{10}(T_{rep} - T_{pulse})] \} \quad (15)$$

The solution of Equations (14) and (15) yields Equations (16) and (17):

$$\alpha = \frac{k_{ex}}{k_{10}} \frac{1 - \exp[-k_{10}(T_{rep} - T_{pulse})]}{1 - \exp(-k_{ex}T_{pulse} - k_{10}T_{rep})} \quad (16)$$

$$\beta = \frac{k_{ex}}{k_{10} + k_{ex}} \frac{1 - \exp[-(k_{10} + k_{ex})T_{pulse}]}{1 - \exp(-k_{ex}T_{pulse} - k_{10}T_{rep})} \quad (17)$$

Next, the average S_1 population during one repetition period is given by (remember that $s_0 + s_1 = s_{tot}$) Equation (18):

$$\bar{s}_1 = \frac{1}{T_{rep}} \int_0^{T_{rep}} dt (s_{tot} - s_0) \equiv \kappa s_{tot} \quad (18)$$

where κ is explicitly found from the above solutions for s_0 as [Equation (19)]:

$$\kappa = \frac{k_{ex}}{k_{\Sigma}} \frac{T_{pulse}}{T_{rep}} + \frac{k_{ex}^2}{k_{\Sigma}^2 T_{rep} k_{10}} \frac{[1 - \exp(-k_{\Sigma} T_{pulse})][1 - \exp(-k_{10} \Delta T)]}{1 - \exp(-k_{10} T_{rep} - k_{ex} T_{pulse})} \quad (19)$$

where the short-hand notations $k_{\Sigma} = k_{ex} + k_{10}$ and $\Delta T = T_{rep} - T_{pulse}$ were used. Next, triplet state dynamics are considered. In a steady-state equilibrium, the average population of the triplet state is balanced by the transition from the triplet state back to the ground state, or [Equation (20)]:

$$k_{isc} \bar{s}_1 \equiv k_{isc} \kappa s_{tot} = k_{ph} (1 - s_{tot}) \quad (20)$$

where k_{isc} and k_{ph} are the intersystem crossing rate and triplet-to-ground-state transition rates, respectively. This yields an expression for the as yet unknown s_{tot} [Equation (21)]:

$$s_{tot} = \frac{k_{ph}}{k_{isc} \kappa + k_{ph}} \quad (21)$$

Finally, the fluorescence rate is given by Equation (22):

$$I_f = \phi_f k_{10} k_{\text{sc}} S_{\text{tot}} = \frac{\phi_f k_{10} k_{\text{sc}}}{1 + (k_{\text{isc}}/k_{\text{ph}})k_{\text{sc}}} \quad (22)$$

where ϕ_f is the fluorescence quantum yield. In the limit of continuous-wave (cw) excitation ($T_{\text{pulse}} = T_{\text{rep}}$), one recovers the standard result [Equation (23)]:

$$I_f = \frac{\phi_f k_{\text{ex}}}{1 + (k_{\text{ex}}/k_{10})(1 + k_{\text{isc}}/k_{\text{ph}})} \quad (23)$$

which can be rewritten, in the generic form, as Equation (24):

$$I_f = \frac{\phi_f k_{\text{ex}}}{1 + k_{\text{ex}}/k_{\text{sat}}} \quad (24)$$

where the optical saturation rate k_{sat} is defined by Equation (25):

$$k_{\text{sat}} = \frac{k_{10}}{1 + k_{\text{isc}}/k_{\text{ph}}} \quad (25)$$

Equations (22) and (19) give the searched-for relation connecting the EID (i.e., k_{ex}) with the EPD (i.e., I_f), so that the final MDF $U(\rho, z)$ can be calculated as the product of the EPD and the CEF.

Results

Figure 1 shows calculated optical saturation curves, that is, the dependence of the fluorescence rate on the average excitation rate $k_{\text{ex}} T_{\text{pulse}}/T_{\text{rep}}$. The excitation rate k_{ex} itself is given by the

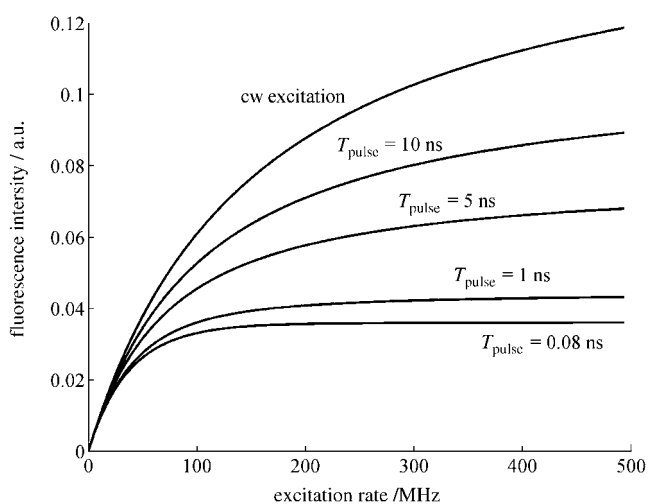


Figure 1. Optical saturation curves for different pulse lengths of the excitation laser. The fluorescing dye was assumed to have an excited-state lifetime of 3.2 ns (Alexa633); the laser pulse repetition rate was 40 MHz. Results for the value $k_{\text{isc}}/k_{\text{ph}} = 1$ are displayed.

product of the molecule's absorption cross-section, σ , multiplied by the excitation intensity, given in photons per area per time. Thus, the average excitation rate is the average rate with

which a molecule would be excited if the exciting light were uniformly distributed in time. In the limit of infinitely short excitation laser pulses, the maximum achievable rate of excitation can only equal the repetition rate of the laser and is much less than the average rate $k_{\text{ex}} T_{\text{pulse}}/T_{\text{rep}}$.

However, by using the average excitation rate as the horizontal axis in Figure 1, it is possible to compare different excitation modes (with respect to pulse length) with the same average excitation intensity. Shown are results for pulsed excitation with a 40 MHz repetition rate and different pulse lengths, so that a pulse length of 25 ns corresponds to cw excitation. The fluorescence lifetime $\tau \approx k_{10}^{-1}$ was assumed to be 3.2 ns, which corresponds to that of Alexa633, and the ratio $k_{\text{isc}}/k_{\text{ph}}$ was set to unity, a value that best fits the measured FCS results below. It is important to note that the displayed curve for the shortest pulse-width of 80 ps is close to the limiting case of an infinitely short pulse-width, thus being basically the same as that for femtosecond excitation, which is widely encountered when using Ti:Sapphire lasers for excitation.

Figure 2 visualizes the impact of increasing optical saturation on the MDF for cw excitation and the same values of τ and $k_{\text{isc}}/k_{\text{ph}}$ as in Figure 1. The MDFs were computed as the direct

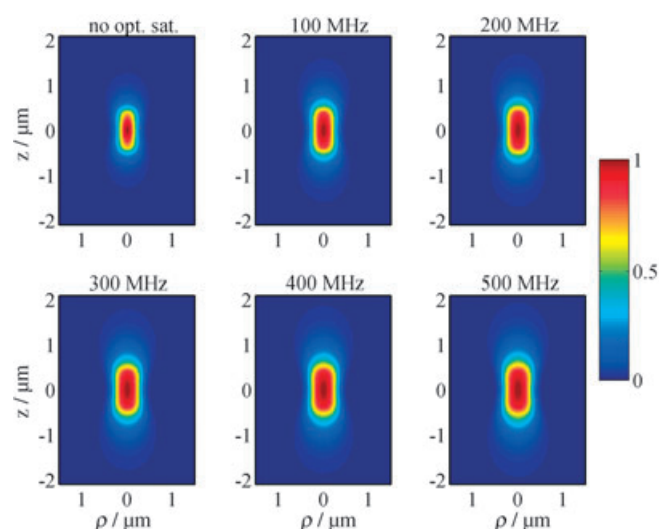


Figure 2. Calculated MDF for six different values of the cw excitation rate. The following model parameters were used: fluorescence lifetime $\tau = 3.2$ ns; ratio of intersystem crossing to triplet state depopulation rate $k_{\text{isc}}/k_{\text{ph}} = 1$; laser beam waist radius of $w_0 = 300$ nm ($1/e^2$ maximum intensity value); numerical aperture of objective $NA = 1.2$; magnification of detection optics $60\times$; pinhole size of $100 \mu\text{m}$ diameter. Shown are six panels for six different excitation rates, where the maximum rate at the $\rho = z = 0$ is indicated on top of each panel. This rate is equal to $2P_0/\pi w_0^2$ where P_0 is the total laser beam power in photons per time per area. The first subplot (top left) shows the MDF in the limit of zero excitation rate (no optical saturation).

product of the fluorescence rate distribution and CEF. The CEF was calculated using Equation (9) for an objective with 1.2 NA and $60\times$ magnification, and for a pinhole size of $100 \mu\text{m}$. The fluorescence rate distribution was obtained assuming excitation with a Gaussian laser beam [see Equation (7)] with a $1/e^2$ beam radius of 300 nm and employing the relationship, Equa-

tion (22), between the fluorescence rate and excitation intensity. The different excitation rates shown at the top of the panels refer to the maximum excitation rate in the center of the detection region, where the excitation rate is equal to $2P_0/\pi\omega_0^2$; P_0 denotes the total laser beam power in units of photons per time. Thus, for a beam waist radius of 300 nm at an excitation wavelength of 635 nm, and for a typical dye extinction value of $10^5 \text{ L mol}^{-1} \text{ cm}^{-1}$, an average excitation rate of 100 MHz corresponds to a total laser beam power of 116 μW . All the MDF distributions shown are normalized to their maximum value, showing the relative probability density of detecting a fluorescence photon from a given position in space. Displayed are only cross-sections of the MDF in the ρ - z -plane; excitation and detection are invariant with respect to rotations around the optical axis. The panels clearly show an enlargement of the effective detection volume with increasing average excitation rate, even in the case of cw excitation shown here where optical saturation has the least impact (see also Figure 1).

Two series of FCS measurements with varying excitation power were performed: one by exciting with a pulsed diode laser, the other by exciting with a cw Kr/Ar-ion laser. Figure 3

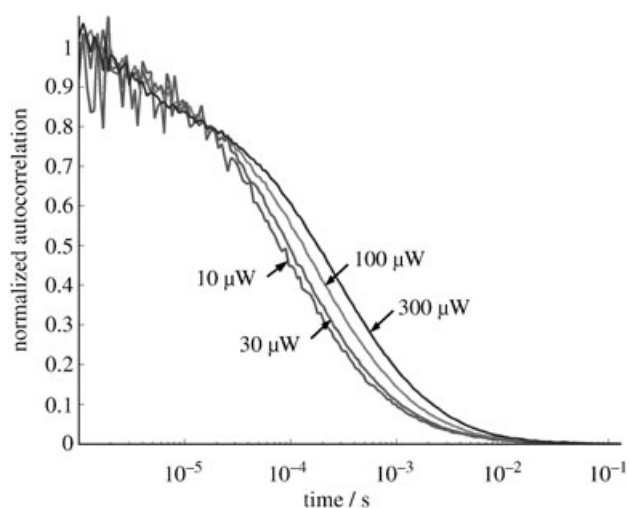


Figure 3. Measured ACFs for four different values of the excitation power (10 μW , 30 μW , 100 μW , and 300 μW) under pulsed excitation (repetition rate 40 MHz, pulse width ~ 80 ps) and at 635 nm excitation wavelength. Higher excitation power shifts the temporal decay of the ACF to longer lag times.

shows the measured and normalized FCS curves obtained with pulsed laser excitation at four different excitation powers. A shift of the temporal decay of the autocorrelation to longer lag times for higher excitation power is clearly visible. To compare the apparent diffusion coefficients of the different FCS curves, they were fitted with the standard model curve given by Equation (26):

$$g(t) = \left[T + (1-T)\exp\left(-\frac{t}{\tau_T}\right) \right] \left[\frac{A}{(1+t/\tau_D)\sqrt{1+\zeta t/\tau_D}} \right] + B \quad (26)$$

where A , B , T , τ_T and τ_D are fitting parameters that are different for each measured curve; whereas ζ is kept constant for all fitted curves. The factor $T+(1-T)\exp[-(k_{\text{ph}}+k_{\text{isc}})t]$ was included to take into account the fast triplet-state dynamics.^[26,27] Although Equation (26) is based on the simplified assumption of a three-dimensional Gaussian shape of the MDF, it fits the data well, and regardless of the physical reasonability of the underlying model, the ratio of the fit parameter τ_D for two different curves will give the correct value of the inverse ratio of the diffusion coefficients. Indeed, for monocomponent samples with normal diffusion behavior, the diffusion-related part of the ACF for two different samples is connected by an affinity transformation, that is, the curves can be transformed into each other by purely stretching/compressing the vertical and horizontal axes. This is a direct result of the exact Equations (4) and (6), showing that only the product of the diffusion coefficient and lag time determines the shape of the diffusion-related part of an autocorrelation curve. Figure 4 shows an exemplary result

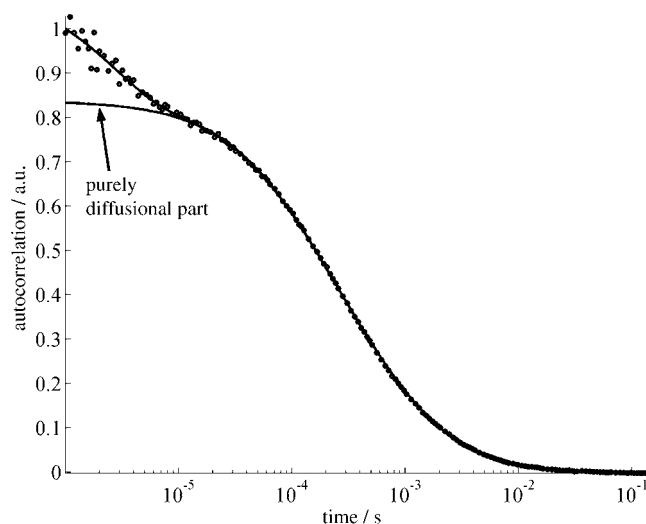


Figure 4. Fitting of the FCS curve measured for 300 μW average excitation power under pulsed excitation. Circles (\circ) are the experimental results; the solid lines (—) show the full fit and the purely diffusional contribution.

of fitting the model curve, Equation (26), against the ACF measured with pulsed excitation at average excitation power of 300 μW . Besides the measured curve and its fit, the diffusion-related part is shown separately. Using the fitted values τ_D , the power dependence of the apparent diffusion coefficient was determined using the diffusion of the 300 μW pulsed-excitation curve as the reference (the ratio of the apparent diffusion coefficients associated with two measurements was determined by $D_1/D_2 = \tau_{D2}/\tau_{D1}$). The resulting dependence of the apparent diffusion coefficient on the excitation power, for both pulsed and cw excitation, is shown in Figure 5 together with theoretical fits. Numerical calculation of the theoretical curves was obtained by calculating the ACF and its dependence on excitation power, as outlined in the theory section, using parameter values equal to those of the experimental setup, assuming additionally a beam waist diameter of the focused

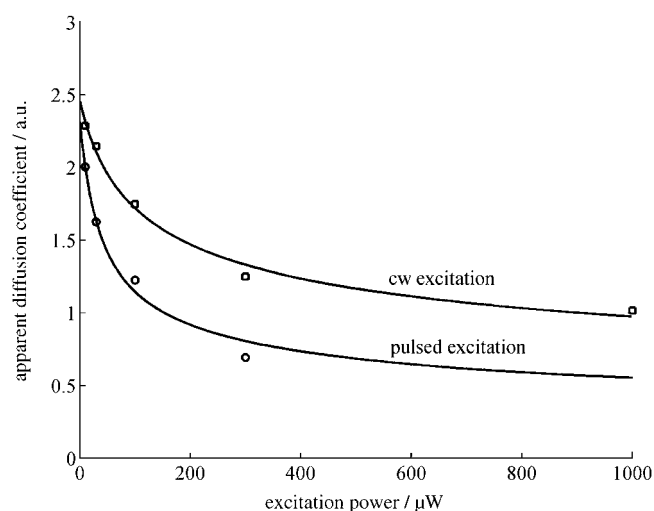


Figure 5. Dependence of the apparent diffusion coefficient on the average excitation power. Circles (○) are experimental results for pulsed excitation, and squares (□) are experimental results for cw excitation; solid lines (—) are the theoretical fits.

laser beam of 300 nm radius ($1/e^2$), as was estimated by scanning single fluorescing molecules that were immobilized on a glass surface. Additionally, it occurred that the experimentally measured dependence of the apparent diffusion coefficient on excitation power could be best reproduced for a ratio of k_{isc}/k_{ph} close to one. One difficulty when comparing the calculated dependence of the apparent diffusion coefficient with the measured one is the uncertainty of knowing the exact excitation intensity within the sample. Since the radius of the laser beam entering the objective is larger than the radius of the back focal aperture of the objective, and because of internal light losses within the objective, the measured total power of the laser beam is larger, by an unknown factor, than the excitation power arriving in the sample. Thus, the fitting of the theoretically calculated curves to the experimental ones was done by an affinity transformation: The horizontal and vertical axes of the theoretical curve were rescaled to best-fit the experimental curve, which resulted in two fitting parameters (two scaling factors). The scaling factor of the vertical axis is of little physical significance because only relative changes of the diffusion coefficient are important. The scaling factor of the horizontal axis gives the relationship between excitation power of the experimental laser beam and the average excitation rate $k_{ex}T_{pulse}/T_{rep}$ as used in the model calculations.

Discussion

The difference between pulsed and cw excitation at the same average excitation power is clearly visible in Figure 5, in which both the experimental results and the model calculations are shown. Even moderately short pulsing of the excitation light dramatically changes the power dependence of the FCS measurement and, thus, the apparent diffusion coefficient. Another important aspect can be seen from Figure 5: The slope of the power dependence for the apparent diffusion coefficient is

largest in the limit of small excitation power. Thus, even measuring the FCS at very small excitation power will not necessarily give power-independent results. Moreover, the statistical accuracy of an FCS measurement roughly scales with the square of the fluorescence rate. Thus, with a tenfold reduction of the excitation power, one would require, roughly, a one-hundred-times-longer measurement time to obtain an FCS curve of comparably good statistical accuracy. This precludes measurements at too small an excitation power. An alternative option for obtaining power-independent results seems to be to record the power dependence of the apparent diffusion coefficient over an extended range of excitation powers (as was done here and is shown in Figure 5) and to extrapolate that dependence towards zero excitation power. However, that necessitates a correct theoretical model, which can be used to extrapolate the measured power-dependence curve correctly. Although we have performed such calculations based on knowledge of the EPD and CEF, the correspondence between the measured and calculated curves is not perfect. Most importantly, the fitted curves for cw and pulsed excitation do not intersect the ordinate at exactly the same point, as they should. This is partially due to the affinity transformation fitting procedure, which allows the scaling factor of the vertical axis to change freely during fitting. There are also several possible physical reasons: i) the neglect of polarization effects in calculating the MDF; ii) possible astigmatism of the focused laser beam due to slight ellipticity of the optical fiber used to deliver the excitation light towards the objective, and due to non-perfect flatness of the dichroic mirror; iii) more complex optical saturation curves due to the non-rectangular shape of the excitation pulses. However, the most important point herein is the demonstration that FCS measurements are very sensitive to optical saturation effects, even—and especially—at low excitation power, and that there is a significant difference of this behavior for cw and pulsed excitation. As clearly demonstrated, the rate of change of the apparent diffusion coefficient on excitation power is largest in the limit of infinitely small excitation power, thus making any correct estimate of true diffusion coefficients by standard FCS extremely difficult.

Experimental Section

The experimental setup has been described in detail elsewhere.^[28] Two different laser sources were used for the experiment: a pulsed diode laser at a wavelength of about 639 nm (PDL 800, PicoQuant), which generated pulses with widths of 50 ps and a 40 MHz repetition rate, and a continuous-wave Kr/Ar-ion laser at wavelength of 647.1 nm (Stabilite 2018, Spectra Physics). The light of either laser was sent through a single-mode glass fiber and subsequently collimated to form a Gaussian profile beam with a beam waist radius of 5 mm. The beam was then focused through an apochromatic water-immersion objective (1.2 NA, 60×, Olympus) into the sample solution. The fluorescence was collected by the same objective (epi-fluorescence setup), and then separated from the excitation light by a dichroic mirror (650 DRLP, Omega Optical). After passing an additional bandpass filter (670DF40, Omega Optical), a tube lens with a 180 mm focal length focused it onto a circular pinhole with a diameter of 100 μm. After the pinhole, the light was split

into two channels and refocused by a 10× objective onto two single-photon avalanche diodes (SPCM AQR-13, Perkin Elmer). Fast electronics (TimeHarp 200, PicoQuant) was used for recording the detected photons in time-correlated time-tagged recording mode.^[28] From these raw data, the autocorrelation curves were calculated by cross-correlating photons from the two different SPADs.^[29] This cross-correlation prevented distortions of the autocorrelation curve due to SPAD after pulsing.^[30]

FCS measurements were performed on a solution ($\approx 10^{-9}$ M) of Alexa633 (Molecular Probes) in bidistilled water. FCS measurement times ranged between 20 min and 1.5 h, depending on the excitation intensity. The excitation power was measured with a power meter (S120 A, Thorlabs) at the back-entry aperture of the objective. Power was adjusted with a gray filter wheel (STA-EAM 2, Laser 2000) and ranged between 1 and 300 μ W for the diode laser, and between 10 μ W and 1 mW for the cw ion laser. All measurements were performed at 20 °C.

Acknowledgements

We thank Martin Böhmer for his technical support, and we are much obliged to Benjamin Kaupp for his generous support of our work. This work was financially supported by the Deutsche Forschungsgemeinschaft (grant EN 297/7), the Deutsche Volkswagenstiftung, and the Humboldt Foundation.

Keywords: diffusion coefficients · fluorescence spectroscopy · fluorescence · optical saturation

[1] D. Magde, E. Elson, W. W. Webb, *Phys. Rev. Lett.* **1972**, *29*, 705–708.

[2] E. L. Elson, D. Magde, *Biopolymers* **1974**, *13*, 1–27.

[3] D. Magde, E. Elson, W. W. Webb, *Biopolymers* **1974**, *13*, 29–61.

[4] N. L. Thompson in *Topics in Fluorescence Spectroscopy*, Vol. 1 (Ed.: J. R. Lakowicz), Plenum Press, New York, **1991**, pp. 337–378.

[5] J. Widengren, Ü. Mets in *Single-Molecule Detection in Solution—Methods and Applications* (Eds.: C. Zander, J. Enderlein, R. A. Keller), Wiley-VCH, Berlin, **2002**, pp. 69–95.

[6] *Fluorescence Correlation Spectroscopy* (Eds.: R. Rigler, E. Elson), Springer, Berlin, **2001**.

[7] P. Schwille, *Cell Biochem. Biophys.* **2001**, *34*, 383–408.

[8] S. T. Hess, S. Huang, A. A. Heikal, W. W. Webb, *Biochem.* **2002**, *41*, 697–705.

[9] O. Krichevsky, G. Bonnet, *Rep. Prog. Phys.* **2002**, *65*, 251–297.

[10] S. Sterrer, K. Henco, *J. Recept. Signal Transduction Res.* **1997**, *17*, 511–520.

[11] R. D. Icenogle, E. L. Elson, *Biopolymers* **1983**, *22*, 1919–1948.

[12] R. D. Icenogle, E. L. Elson, *Biopolymers* **1983**, *22*, 1949–1966.

[13] D. Magde, *Q. Rev. Biophys.* **1976**, *9*, 35–47.

[14] P. Schwille, J. Bieschke, F. Oehlenschläger, *Biophys. Chem.* **1997**, *66*, 211–228.

[15] J. Widengren, R. Rigler, *Cell. Mol. Biol.* **1998**, *44*, 857–879.

[16] C. Eggeling, J. Widengren, R. Rigler, C. A. M. Seidel, *Anal. Chem.* **1998**, *70*, 2651–2659.

[17] J. Mertz, *Eur. Phys. J. D* **1998**, *3*, 53–66.

[18] N. Niesner, W. Roth, K. H. Gericke, *ChemPhysChem* **2004**, *5*, 678–687.

[19] J. Enderlein, I. Gregor, D. Patra, J. Fitter, *Current Pharmaceutical Biotechnol.* **2004**, *5*, 155–161.

[20] G. Nishimura, M. Kinjo, *Anal. Chem.* **2004**, *76*, 1963–1970.

[21] K. Berland, G. Shen, *Appl. Opt.* **2003**, *42*, 5566–5576.

[22] R. Kühnemuth, C. A. M. Seidel, *Single Mol.* **2001**, *2*, 251–254.

[23] M. Böhmer, M. Wahl, H. J. Rahn, R. Erdmann, J. Enderlein, *Chem. Phys. Lett.* **2002**, *353*, 439–445.

[24] J. Enderlein, *Opt. Lett.* **2000**, *25*, 634–636.

[25] *Handbook of Mathematical Functions* (Eds.: M. Abramowitz, I. A. Stegun), Harry Deutsch, Thun, Frankfurt am Main, **1984**.

[26] J. Widengren, P. Schwille, *J. Phys. Chem. A* **2000**, *104*, 6416–6428.

[27] J. Widengren, Ü. Mets, R. Rigler, *J. Phys. Chem.* **1995**, *99*, 13368–13379.

[28] M. Böhmer, F. Pampaloni, M. Wahl, H. J. Rahn, R. Erdmann, J. Enderlein, *Rev. Sci. Instrum.* **2001**, *72*, 4145–4152.

[29] M. Wahl, I. Gregor, M. Patting, J. Enderlein, *Opt. Express* **2003**, *11*, 3583–3591.

[30] M. Höbel, J. Ricka, *Rev. Sci. Instrum.* **1994**, *65*, 2326–2336.

Received: July 8, 2004

Early View Article
Published online on December 9, 2004